Radiation Measurements 114 (2018) xxx–xxx

Contents lists available at ScienceDirect

Radiation Measurements

journal homepage: www.elsevier.com/locate/radmeas

Detecting and quantifying uranium-series disequilibrium in natural samples for dosimetric dating applications

S.A. Abdualhadi[a], B. Mauz[b,c,*], S.D.T. Joss[a], P.J. Nolan[a]

[a] School of Physical Sciences, University of Liverpool, Liverpool L69 7ZF, UK
[b] School of Environmental Sciences, University of Liverpool, Liverpool L69 7ZT, UK
[c] School of Geology and Geography, University of Salzburg, 5020 Salzburg, Austria

ABSTRACT

Isotopic fractionation is a process that may occur in natural aquatic environments. Samples originating from these open-system environments may contain radioisotopes with activity ratios between daughter and mother nuclide being not at unity. For the purpose of dosimetric dating, small deviations from unity may have negligible effect, but the mobility of ^{226}Ra and ^{234}U over longer time scales affects the accuracy of the dating result. Here we use the Canberra LabSOCS model in association with a standard 60 mm diameter BEGe detector in a 50 mm thick graded lead shield to carry out gamma spectroscopic measurements on the ^{238}U decay series in a series of environmental samples. These samples were characterised in terms of density, filling height and chemical composition and peak interferences were corrected using the gf3 software. The model calculations have been shown to be in agreement with experimental transmission measurements taken with point sources and with results from standard IAEA materials and through a comparison with ICP-MS measurements. The results presented show excellent agreement between outputs from model and independent control measurements. This suggests that the method presented here is robust and allows quantifying and correcting isotopic fractionation using readily available gamma spectrometric setup and software.

1. Introduction

Many of the naturally occurring radioactive elements are members of radioactive decay chains. These chains originate from parent nuclides with very long half-lives, ^{238}U (4.47×10^9 a), ^{235}U (7.04×10^8 a) and ^{232}Th (1.4×10^{10} a) and end with the stable nuclide of lead, ^{206,207,208}Pb (National Nuclear Data Centre, NNDC). In any undisturbed natural material, a state of secular equilibrium occurs between the parent nuclide and its daughter products. However, nature sedimentary processes involving water can cause isotopic fractionation of the elements resulting in a state of disequilibrium between the parent nuclide and its daughters in the chain (Ivanovich and Harmon, 1992) by which the activity ratio between parent and daughter is either above or below the unity. In natural samples isotope fractionation is negligible for all radioisotopes with short half-lives. For some U daughters however the disturbance can be significant resulting in inaccurate dosimetric age estimates (e.g., Guibert et al., 2009). To quantify a disequilibrium within the U-chain, the activity concentration of each radionuclide in the chain must be determined accurately. Among the instrumental methods used for this purpose, gamma spectrometry is often the method of choice in dosimetric dating because sample preparation and data processing are simple and well-established. To use the technique for the purpose of quantifying U-chain disequilibrium is however challenging. It requires the accurate determination of low energy gamma rays which are affected by peak interference and self-absorption within the sample. The issue is well-known in nuclear physics and industry where it is solved through a combination of experimental measurements and computer simulations (e.g. Šoštarić et al., 2016). For the application of dosimetric dating in environmental science the issue is known (Krbetschek et al., 1994; Olley et al., 1996) but often not solved due to the nontrivial nature of the problem and the complicated measurement requirements. Guibert et al. (2009) proposed to use the variance of the concentrations of each radioelement in the different samples. Lahaye et al. (2012) calculated the concentration of the uranium radioisotopes as a function of the time elapsed since the event of alteration, assuming a linear uptake of ^{234}U.

This study developed a new procedure to fully address peak interference and self-absorption for dosimetric dating applications. The procedure is designed for a BEGe germanium gamma-ray detector due to its enhanced energy resolution at low gamma-ray energy (i.e. < 100 keV)

* Corresponding author.School of Environmental Sciences, University of Liverpool, Liverpool L69 7ZT, UK.
E-mail address: mauz@liverpool.ac.uk (B. Mauz).

https://doi.org/10.1016/j.radmeas.2018.04.011
Received 7 June 2017; Received in revised form 18 April 2018; Accepted 18 April 2018
Available online 20 April 2018
1350-4487/

and good efficiency over a wide range of gamma-ray energies from 3 keV to above 2 MeV. The efficiency of the system is determined using the detailed properties of each sample using the LabSOCS model. This allows accurate massic activity measurements to be made over a wide range of gamma-ray energies where 'massic' refers to the mass of the sample.

2. Peak interference and self-absorption

When investigating U-chain isotope fractionation the gamma ray energies of ^{210}Pb (46.5 keV) and ^{234}Th (63.3 keV; 92.6 keV) and ^{226}Ra (186.4 keV) are of interest. Quantifying the photon emission of these energies in a given sample is challenging due to (i) interference of peaks of various gamma-emitting radioisotopes, in particular at the energy of 92 keV and 186 keV peaks and (ii) significant attenuation within the sample. At 186 keV the gamma peak of ^{226}Ra (186.4 keV) is interfered by ^{235}U (185.7 keV) and at 92 keV the gamma peak of ^{234}Th is interfered by other x-ray and gamma peaks including the 93.3 keV thorium line (Huy and Luyen, 2005). De Corte et al. (2005) address the issue by calculating the ^{235}U (185.7 keV) peak area from the ^{234}Th peak at 63.3 keV assuming that ^{238}U/^{235}U is constant.

The attenuation of gamma-ray energies (particularly < 100 keV) is a function of detector geometry, measurement geometry (Fig. 1) and the chemical composition and density of the sample. It can be described as $e^{-\mu x}$ which is the probability of a gamma photon to travel the distance x with a linear attenuation coefficient μ. Most studies determine the gamma-ray energy dependent sample specific attenuation coefficient μ_s through a combination of experimental and computer-based models (e.g., Šoštarić et al., 2016; Bruggeman et al., 2016; Huy et al., 2013) or through theoretical calculations of self-attenuation correction factors (Appleby et al., 1992; Barrera et al., 2017). The computer-based approach includes Monte-Carlo (MC) simulation (e.g., Huy et al., 2013) that often requires μ_s to be known. The experimental approach includes transmission measurements with collimated sources by which the sample's efficiency at low energies (e.g. < 100 keV) is measured directly, or a comparison with an uranium ore (U_3O_8) containing reference material of a given density by which energy-specific correction factors (Hasan et al., 2002) are determined.

For the purpose of dosimetric dating, transmission measurements are regarded as not suitable as they require specialised equipment and point sources which are not readily available to most laboratories. Instead, MC simulation through an existing software code seems more appropriate, in particular as this approach allows the use of pre-existing measurement geometries. However, chemical composition and density of the sample must be known which is a challenge because some techniques do not allow determining the full composition of samples or are not accurate enough for the purpose of determining μ_s. Suitable techniques are atomic absorption spectroscopy, mass-spectrometry, x-ray fluorescence and Scanning Electron Microscopy coupled with Energy Dispersive Spectroscopy.

To calculate the massic activity (Bq·kg^{-1}) of a radionuclide the net area of the peak, the efficiency of the detector, the sample mass and the emission probability of the radionuclide are taken into account:

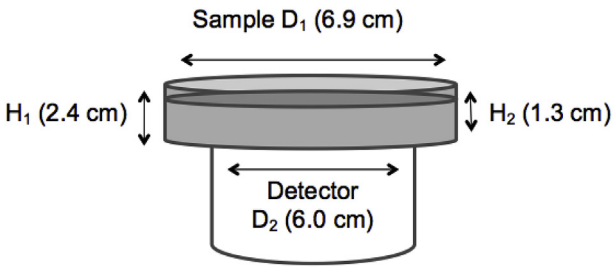

Fig. 1. The cylindrical measurement geometry used in this study. D_1 and D_2 are diameters of sample container and detector, respectively; $H_1$and H_2 is height of sample container and sample, respectively.

Table 1
Gamma-ray energies and associated emission probability per decay used for determining activity concentrations (National Nuclear Data Centre). For 63.3 keV the emission probability is the sum of the double gamma-ray at 62.9 keV and 63.3 keV (0.016%, 3.7% respectively). For 92.6 keV the emission probability is the sum of the double gamma-ray at 92.4 keV and 92.8 keV (2.13%, 2.10% resepctively).

Radionuclide	E_γ (keV)	Emission probability (%)
^{234}Th	63.3	3.72
	92.6	4.23
^{226}Ra	186.2	3.64
^{214}Pb	295.2	18.42
	351.9	35.60
^{214}Bi	609.3	45.49
	1120.2	14.92
	1764.4	15.30
^{210}Pb	46.5	4.25

$$A = N/t\varepsilon Bm$$

where N is net area of the photopeak, t is the counting time of measurements (s), m is the mass of the sample (kg), ε is the counting efficiency at a specific energy and B is the gamma-ray emission probability.

^{238}U activity is determined through its immediate daughter ^{234}Th (in secular equilibrium due to the half-life of 24.1 days (Dowdall et al., 2004; De Corte et al., 2005) with its gamma rays of 63.3 keV and 92.6 keV. The peak of 92.6 keV interferes with other x-ray and gamma peaks including the 93.3 keV K x-ray thorium line (Huy and Luyen, 2005). ^{226}Ra is identified through its 186.2 keV emission which interferes with the 185.7 keV gamma ray of ^{235}U and through its granddaughters ^{214}Pb (351.9 keV, 295.2 keV), ^{214}Bi (609.3 keV, 1120.3 keV, 1764.5 keV) and ^{210}Pb (46.5 keV) which reach secular equilibrium with ^{226}Ra within one month in a closed system. For emission probabilities see Table 1.

3. Experimental design

3.1. Instrumentation

The measurements were performed using a Canberra Broad Energy Germanium detector (BEGe2825 model) of 60 mm diameter and 25 mm thickness. The detector was enclosed in a 5 cm thick cylindrical lead shield graded with 1 mm copper and 1 mm tin to absorb the lead-derived X-rays. The detector was connected to a Canberra Lynx data acquisition system with a 14-bit 80 MHz flash ADC and an internal trigger. This system exhibits very good energy resolution (Fig. 2) and allows energy lines of the low-energy range to be sufficiently well separated for quantitative analyses (Fig. 3).

3.2. Efficiency calibration

The accurate determination of the detector efficiency at low gamma-ray energies is crucial when investigating disequilibrium in environmental samples, particularly when using the 46.5 keV from ^{210}Pb and the 63.3 keV and 92.6 keV from ^{234}Th gamma rays from ^{238}U decay series (Joshi, 1987). A common approach for efficiency calibration is measuring a reference material with known activity that exhibits multiple energy transitions (Fig. 4). To account for the drop in efficiency at 63 keV and below (Fig. 4) caused by absorption within the sample's material matrix the Canberra LabSOCS module (Laboratory Sourceless Object Calibration Software) was employed (Canberra LabSOCS). This software calculates the gamma-ray efficiency as a function of gamma-ray energy by taking into account the specific characteristics of the individual detector and the user-defined input parameters such as the measurement geometry, the sample's chemical composition and its density. LabSOCS includes the characterization of

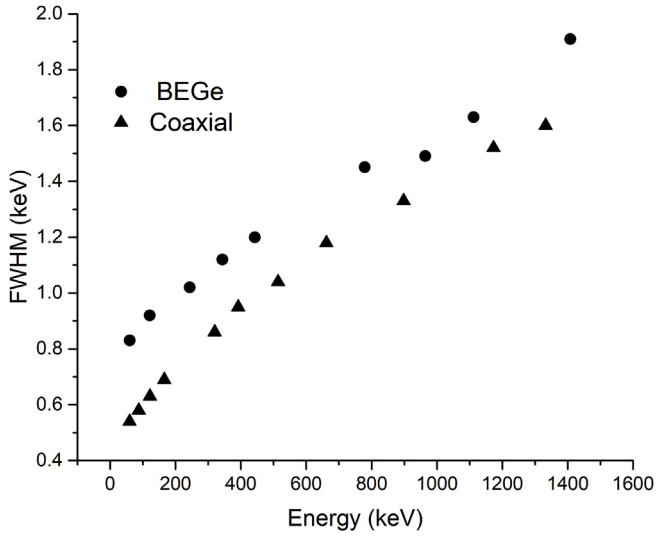

Fig. 2. Full-Width Half-Maximum (FWHM) as a function of gamma-ray energy for a Broad-Energy Germanium (BEGe) detector and a Coaxial Ge detector of the same diameter.

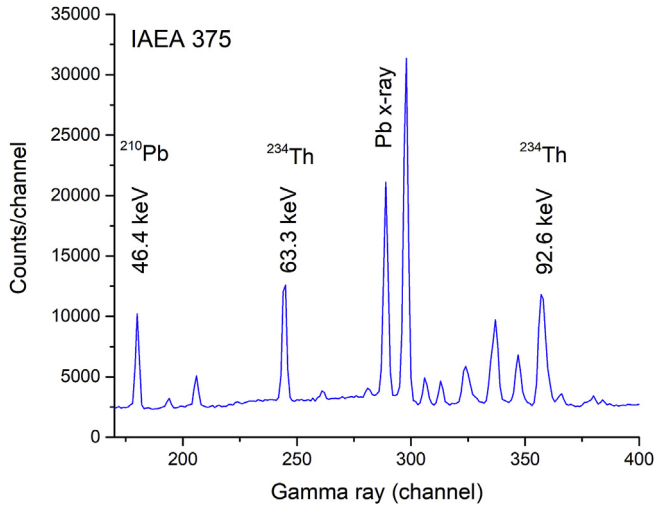

Fig. 3. The low-energy part of the gamma spectrum of the IAEA-375 standard material collected by the Broad-Energy Ge (BEGe) detector.

the germanium detector deduced from high-precision source measurements and a simulation optimization produced with a Monte Carlo transport code. This provides the vacuum-point efficiencies unique to the detector in use, and the software then determines the attenuation correction for the specific measurement geometry for each sample to be measured.

All input parameters for the sample and detector are stored and a report for the efficiency calibration is performed once the user runs the LabSOCS software.

3.3. Peak fitting and nuclear data

The *gf3* peak fitting software (Radford, 2000) was used to separate the energy lines 92.6 keV and 93.3 keV using least square fitting designed for germanium detectors. For other, well-separated peaks, the peak area can be determined using a Gaussian shape. The peak area (N) for each gamma ray is then used to calculate the activity using the approach described in section 2. The activity of ^{226}Ra was deduced by subtracting the ^{235}U component from the 186 keV line assuming the natural abundance of ^{238}U and ^{235}U (99.27% and 0.725%, respectively)

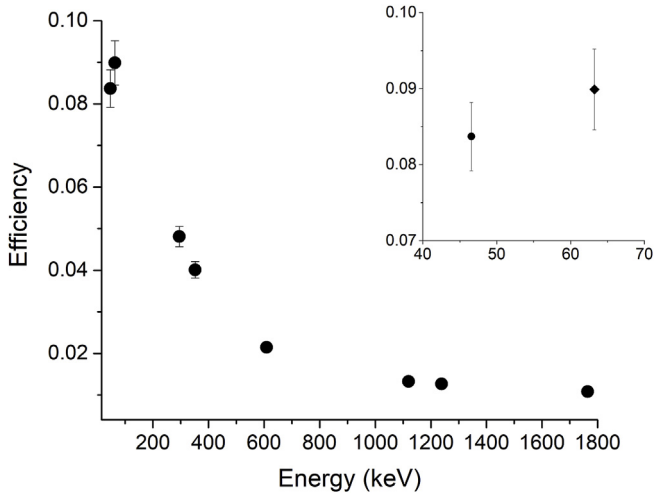

Fig. 4. The efficiency of the BEGe detector for the standard material IAEA-312. The inset shows the drop of efficiency below 100 keV caused by self-absorption. The axes of the inset are the same.

and their half-lives (4.47×10^9 years and 7.04×10^8 years, respectively). Coincidence summing affecting the lines of 609.3 keV and 1120.3 keV in ^{214}Bi was found to result in change of less than 2% due to the relatively low detection efficiency of the system used. The gamma-ray energies and decay branching were obtained from the National Nuclear Data Centre evaluation (see NNDC for reference).

3.4. Samples, sample preparation and analyses

Samples originating from a wide spectrum of natural environments (Table 2) were selected to test the variations in the parameters that can affect the efficiency.

The sample preparation included drying at 105 °C and subsequent cooling in a low-pressure chamber before packing in an air-tight cylindrical container (Fig. 1) using silicon gel and plastic tape around the lid. Measurement began after around 7 half-lives of ^{222}Rn when secular

Table 2
Samples used in this study, their origin and chemical composition. Elements were determined using XRF. The uncertainty of this technique is typically < 5% for Al, K, P, S, Cl, Ca, Fe, Mn, Ti, Rb, Sr and Zr and < 10% for Na, Mg, Cr, V and Ba.

Sample	389	396	516	523	524	Nussi
Origin	49.58N 15.20E	18.41S 16.15E	15.33S 128.40E	18.41S 16.15E	18.41S 16.15E	49.18N 8.42E
Element (%)						
O + C	51.90	53.25	48.88	56.19	55.99	18.66
Si	41.54	20.37	32.97	22.48	18.92	46.47
Al	3.27	2.50	5.81	1.54	2.13	6.87
P	0.01	0.05	0.03	0.05	0.04	0.09
S	0.01	0.10	0.01	–	–	–
Ca	0.28	15.88	1.50	17.48	19.33	18.66
Mg	0.45	2.61	1.37	2.48	3.21	3.20
Cl	0.04	0.38	0.03	0.07	–	–
Na	0.50	3.89	1.00	2.42	2.24	0.99
K	1.30	1.40	1.95	0.76	0.91	1.35
Fe	0.85	0.61	4.19	0.52	0.75	2.19
Mn	0.02	0.03	0.04	0.02	0.02	0.07
Ti	0.15	0.11	0.54	–	–	0.37
Ba	0.03	0.16	0.03	0.11	0.12	–
Cr	–	–	0.01	–	–	–
V	–	–	0.01	–	–	–
Rb	0.01	–	0.01	–	–	–
Sr	0.01	0.22	0.01	0.20	0.17	–
Zr	0.02	0.01	0.03	0.01	0.01	–

equilibrium with ^{226}Ra was achieved. X-ray fluorescence was used to determine the chemical composition of the samples (Table 2). Light elements (C and O) were calculated through standard stochastic formula assuming their occurrence as oxide and carbonate; Sodium (Na) was estimated through repeated measurements. The sample density was calculated from mass and volume measurements.

3.5. Assumptions and uncertainties

The approach assumes a homogeneous distribution of radionuclides in the sample and isotropic emission of the gamma radiation. Uncertainties in the measured net areas of the spectrum are derived from counting (Poisson-) statistics accounting for background subtraction. Efficiency uncertainties were determined in the LabSOCS model using the measurement uncertainties in the sample geometry (typically 0.2 mm in a filling height of 11–15 mm), composition and density determinations. Uncertainties in the efficiency resulting from the sample diameter measurement are negligible as the diameter can be measured more accurately. Uncertainties in the decay branching ratios were taken from the literature (NNDC). All the uncertainties were combined to give the combined standard uncertainty. The standard combined uncertainty is reported in all tables and figures except Fig. 9.

3.6. Comparison between experimental and modelled results

The reliability of the procedure described above was checked by (1) testing it using a well-described material (IAEA reference material) and by (2) comparing its results with results obtained from transmission and from ICP-MS measurements. Transmission measurements were carried out using four gamma-ray point sources that emit in the energy range 31 keV–121 keV, hence as close as possible to the low-energy transition energies of interest. These sources were collimated and positioned at 10 cm distance from the detector window (see geometry in Fig. 1). The detector efficiency was measured with and without the samples placed on the detector both experimentally and in the model. ICP-MS was chosen as an independent method for comparison due to its high precision. The accuracy of the ICP-MS was checked using USGS rock standards and synthetic matrix standards to lie within the typical accuracy range of 3–5%, based on repeated analysis throughout the batch run. Where appropriate, the comparison was facilitated by converting massic activities (Bq kg^{-1}) into activity concentrations (μg g^{-1}) using the atomic weight, half life and Avogadro constant for Uranium.

4. Results and discussion

4.1. Sample height and diameter

Variations in sample height above the detector affect the detection efficiency. To quantify this the full-energy peak efficiencies were modelled (Fig. 5) for a reasonable range of sample heights (ca 1.1–1.5 cm) within the set measurement geometry. The difference in efficiency remains almost constant for energies > 150 keV and increases for energies < 150 keV (see inset in Fig. 5) highlighting the importance of this parameter on the efficiency. For this work uncertainty in the height measurement result in an uncertainty of less than 2% for the modelled efficiency for the low-energy gamma rays (i.e. 46, 63 and 92 keV).

4.2. Density

To assess the effect of density on the detection efficiency the full-energy peak efficiencies were modelled as a function of different densities (Fig. 6) which were adopted from calculated sample densities. As expected, the absorption of low-energy gamma rays increases with increasing density of the material. The resulting uncertainty in the efficiency is less than 0.5% for the low-energy gamma rays (i.e. 46, 63 and 92 keV).

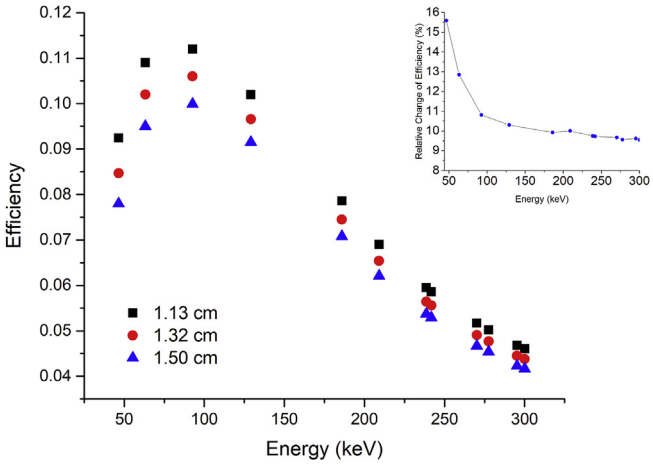

Fig. 5. The effect of sample height on the modelled detection efficiency. The sample 396 was used with density and chemical composition kept constant. Inset shows the relative change of efficiency as a function of energy.

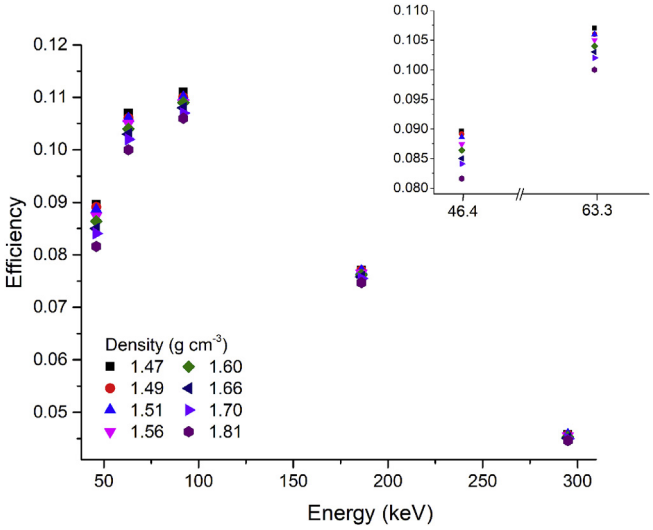

Fig. 6. Modelled efficiencies for one of the samples (396) with varied density, but constant thickness and chemical composition. Inset highlights the density effect on low gamma energies (same data). The axes of the inset are the same.

4.3. Chemical composition

For investigating the influence of the chemical composition the LabSOCS default materials (Table 3) and one of our samples (396, see Table 2) were compared (Fig. 7). The main difference between these materials is the presence (or absence) of higher Z elements such as Fe, K, Na and Ca. Fig. 7 shows that these elements affect the attenuation of lower-energy gamma rays. At 46 keV the detection efficiency was reduced by 8% with 10% of the material being these four elements.

4.4. Comparison with results from transmission, IAEA standard materials and ICP-MS measurements

Modelled and experimentally determined efficiencies of two samples using the transmission measurements are shown in Fig. 8. Within error margins (~2% experimentally) there is a good agreement between model and experiment. The comparison between results from this study and from the independent analyses (IAEA standard materials and ICP-MS) is shown in Fig. 9. In both cases the results agree within error margins.

Table 3
Chemical composition (%) of LabSOCS default material shown in Fig. 7.

Material	Element	%
Dirt1	H	2.20
	O	57.50
	Al	8.50
	Si	26.20
	Fe	5.60
Dirt2	H	1.10
	O	55.80
	Al	7.20
	Si	31.10
	C	1.20
Drydirt	H	0.36
	O	49.62
	Al	7.10
	Si	27.38
	Fe	4.04
	C	2.14
	Na	0.84
	Mg	1.60
	K	2.37
	Ca	4.21
	Ti	0.34

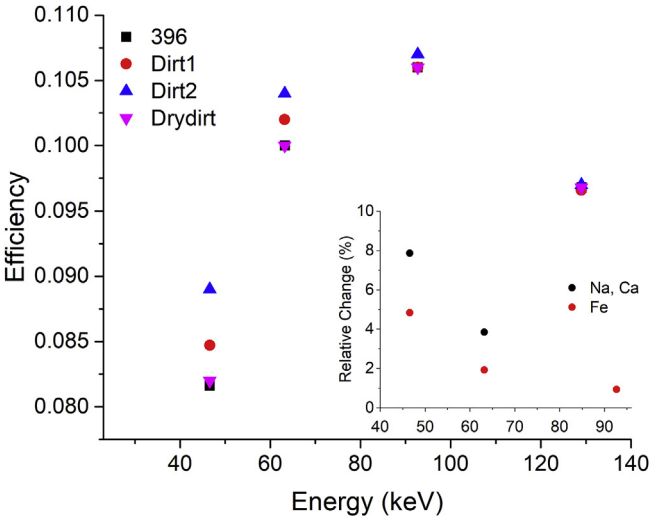

Fig. 7. Modelled efficiency for different chemical compositions (sample height and density kept constant). Dirt samples are default examples provided by LabSOCS software. Inset highlights the impact of higher-Z elements Na, Ca and Fe on the efficiency.

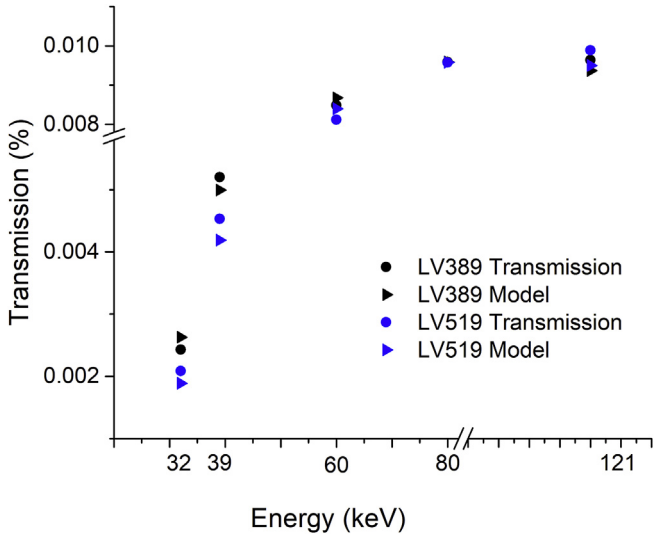

Fig. 8. Comparison between experimental efficiency measurements and modelled results for samples 389 and 519. The uncertainty of the experiment is ~2%; for the sake of clarity relevant error bars are omitted. For details on the transmission measurements including uncertainties see sections 3.6 and 4.4.

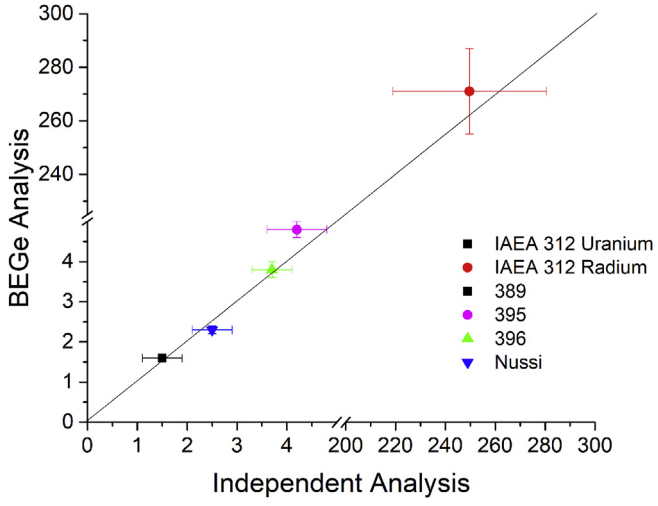

Fig. 9. Results from independent analyses for Uranium (ug g^{-1}) plotted against this study's results. The former originate from IAEA 312 certificate and from ICP-MS measurements. Two sigma error bars are plotted for all data points to be in line with the uncertainties quoted for IAEA standard materials.

4.5. Standard uncertainties

The efficiency is modelled for each sample based on the sample-specific parameters. The uncertainties in the final efficiency depend on the accuracy with which these parameters are determined. The uncertainties in the net areas of the spectrum measured for each gamma transition were typically 5% for the gamma rays below 100 keV and < 2% for higher energy gamma rays. For the activities derived from gamma-ray energies below 100 keV (e.g. ^{234}Th) the overall uncertainty was in the range 6–8%. For activities derived from higher energy gamma-rays the uncertainty was typically 3%.

4.6. Massic activities

The experimental results for the massic activities of the radionuclides ^{234}Th, ^{226}Ra, ^{214}Pb, ^{214}Bi and ^{210}Pb are listed in Table 4. The massic activities of ^{234}Th seem to be higher for the 63.3 keV peak than for the 92.6 keV peak (Fig. 10) possibly due to the attenuation correction, which is higher for 63 keV than for 93 keV. However, when accounting for the uncertainties the results are in agreement confirming the reliability of the efficiency determination for a region of the spectrum where the effects of absorption vary greatly between samples and between energies. Fig. 11 and Table 4 show the measured massic activities which indicate the degree of the radioactive disequilibrium based on the difference in activity concentration between ^{234}Th and ^{226}Ra. The activities of these two radionuclides are in agreement in samples 389 and 519 but disagree in samples 396, 523 and 524 by up to 25 Bq kg^{-1}. The disequilibrium in the latter samples is expressed by the increased activity of ^{226}Ra which suggests excess radium entering the sample's sedimentary environment through water at some moment during burial. ^{226}Ra is the most mobile radionuclide in terrestrial natural systems whereas ^{234}U typically causes disequilibrium in marine systems as shown by its activity ratio of 1.14 with its mother nuclide.

Of all the samples measured in this study, the samples 396, 523 and 524 were found to be in state of secular disequilibrium indicated by the ^{226}Ra/^{234}Th ratio while the short-lived radioisotopes are in equilibrium with their parent ^{226}Ra (Table 4). This type of disequilibrium suggests

Table 4
Massic activities (Bq kg^{-1}) of the relevant radionuclides from ^{238}U decay series of 5 samples tested in this study.

Sample	^{234}Th	^{226}Ra	^{214}Pb	^{214}Bi	^{210}Pb	^{226}Ra/^{234}Th
389	18.4 ± 2.4	13.9 ± 3.1	16.8 ± 0.6	16.6 ± 0.7	15.9 ± 2.6	0.75 ± 0.19
396	45.4 ± 2.7	70.2 ± 4.2	79.7 ± 2.4	75.1 ± 1.9	76.4 ± 5.6	1.55 ± 0.13
519	34.3 ± 3.0	37.3 ± 3.5	28.7 ± 1.1	25.9 ± 1.1	28.3 ± 3.5	1.09 ± 0.14
523	80.2 ± 4.8	97.9 ± 6.0	113.2 ± 3.3	112.2 ± 2.6	96.7 ± 7.5	1.22 ± 0.13
524	62.4 ± 4.8	82.4 ± 5.3	97.4 ± 2.9	87.1 ± 2.2	80.5 ± 6.4	1.32 ± 0.14

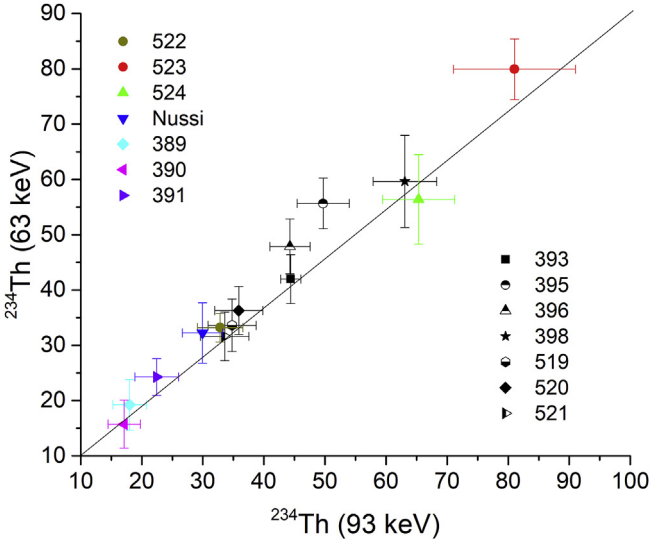

Fig. 10. The ^{234}Th massic activity calculated from the 63.3 keV and the 92.6 keV peak for all samples analysed in this study. The 1:1 line is shown for comparison.

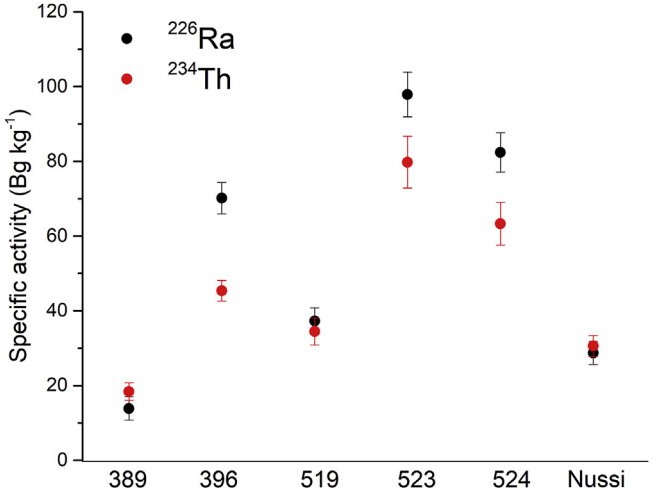

Fig. 11. The ^{234}Th and ^{226}Ra massic activities in some of the samples analysed.

post-depositional uptake of Radium which is typical for terrestrial environments experiencing fluctuation groundwater levels.

5. Conclusions

A standard 60 mm diameter BEGe detector in a 50 mm thick graded lead shield has produced high-quality gamma spectroscopic measurements on the ^{238}U decay series. The excellent low-energy resolution of this type of detector results in improved sensitivity for measurements of the low-energy gamma rays found in this decay series. The efficiency of the system for the range of gamma rays used has been calculated for each sample using the Canberra LabSOCS model. The results show different efficiencies, especially for low energy gamma rays arising from differences in the sample geometry, density and chemical composition. This allows the differences between samples to be accounted for when calculating the massic activities of the nuclides found in the samples taken from a range of different environments. The model calculations were confirmed using a series of experimental measurements carried out with a series of transmission measurements taken with point source, results from standard IAEA materials and a comparison with ICP-MS measurements. The results presented show that in two of the five samples tested the decay chain is in secular equilibrium, while for the other three samples there is evidence for disequilibrium. This is seen through an increase in the massic activity for ^{226}Ra and its decay products.

Acknowledgments

We would like to thank John Boyle for advice concerning the XRF measurements and Peter Appleby for discussions of the results. We would like to thank the University of Cambridge for ICP-MS analysis for some of the samples. Funding was obtained from The Ministry of Higher Education and Scientific Research and the University of Azzaytuna in Libya through the studentship S.A. Abdualhadi_700.

References

Appleby, P.G., Richardson, N., Nolan, P.J., 1992. Self-absorption correction for well-type germanium detectors. Nucl. Instrum. Meth. Phys. Res. B71, 228–233.
Barrera, M., Suarez-Llorens, A., Casas-Ruiz, M., Alonso, J.J., Vidal, J., 2017. Theoretical determination of gamma spectrometry systems efficiency based on probability functions. Application to self-attenuation correction factors. Nucl. Instrum. Meth. Phys. Res. 854, 31–39.
Bruggeman, M., Verheyen, L., Vidmar, T., Liu, B., 2016. Assessing sample attenuation parameters for use in low-energy efficiency transfer in gamma-ray spectrometry. Appl. Radiat. Isot. 109, 547–550.
Canberra LabSOCS application note. Available at: http://canberra.com/literature/application-notes.asp.
De Corte, F., Umans, H., Vandenberghe, D., De Wispelaere, A., Van den Haute, P., 2005. Direct gamma-spectrometric measurement of the ^{226}Ra 186.2 keV line for detecting ^{238}U/^{226}Ra disequilibrium in determining the environmental dose rate for the luminescence dating of sediments. Appl. Radiat. Isot. 63, 589–598.
Dowdall, M., Selnaes, G., Gwynn, J.P., Davids, C., 2004. Simultaneous determination of Ra226 and U238 in soil and environmental materials by gamma-spectrometry in the absence of radium progeny equilibrium. J. Radioanal. Nucl. Chem. 261, 513–521.
Guibert, P., Lahaye, C., Bechtel, F., 2009. The importance of U-series disequilibrium of sediments in luminescence dating: a case study at the Roc de Marsal Cave (Dordogne, France). Radiat. Meas. 44, 223–231.
Hasan, M., Bódizs, D., Czifrus, Sz, 2002. A simplified technique to determine the self-absorption correction for sediment samples. Appl. Radiat. Isot. 57, 915–918.
Huy, N.Q., Binh, D.Q., An, V.X., Loan, T.T.H., Can, N.T., 2013. Self-absorption correction in determining the ^{238}U activity of soil samples via 63.3 keV gamma ray using MCNP5 code. Appl. Radiat. Isot. 71, 11–20.
Huy, N.Q., Luyen, T.V., 2005. A method to determine ^{238}U activity in environmental soil samples by using 63.3 kev-photopeak-gamma HpGe spectrometer. Appl. Radiat. Isot. 61, 1419–1424.
IAEA-375, https://nucleus.iaea.org/rpst/Documents/rs_iaea-375.pdf.
IAEA-312, https://nucleus.iaea.org/rpst/Documents/rs_iaea-312.pdf.
Ivanovich, M., Harmon, R.S., 1992. Uranium-series Disequilibrium: Applications to Earth, Marine, and Environmental Sciences. Clarendon Press, Oxford, pp. 910.

Joshi, S.R., 1987. Nuclear spectrometric determination of uranium isotopes without use of radiochemical yield monitors. Nucl. Instrum. Meth. Phys. Res. 254, 349–354.
Krbetschek, M.R., Rieser, U., Zöller, L., Heinicke, J., 1994. Radioactive disequilibria in palaeodosimetric dating of sediments. Radiat. Meas. 23, 485–489.
Lahaye, C., Guibert, P., Bechtel, F., 2012. Uranium series disequilibrium detection and annual dose determination: a case study on Magdalenian ferruginous heated sandstones (La Honteyre, France). Radiat. Meas. 47, 786–789.
National Nuclear Data Centre (NNDC), Chart of nuclides, Brookhaven Natl. Lab., available at: https://www.nndc.bnl.gov/chart/ (accessed on March 1st 2017). .
Olley, J.M., Murray, A.S., Roberts, R.G., 1996. The effects of disequilibria in the uranium and thorium decay chains on burial dose rates in fluvial sediments. Quat. Geochronol. 15, 751–760.
Radford, D.C., 2000. Notes on the use of the program GF3, Oak ridge National laboratory. available at: http://radware.phy.ornl.gov/gf3, Accessed date: 2 January 2017.
Šoštarić, M., Babić, D., Petrinec, B., Zgorelec, Ž., 2016. Determination of gamma-ray self-attenuation correction in environmental samples by combining transmission measurements and Monte Carlo simulations. Appl. Radiat. Isot. 113, 110–116.